Proposals and analysis of Space Vector-based Phase-Locked-Loop techniques for synchrophasor, frequency and ROCOF measurements

Roberto Ferrero, *Senior Member, IEEE*, Paolo Attilio Pegoraro, *Senior Member, IEEE*, Sergio Toscani, *Senior Member, IEEE*

***Abstract*—Space Vector (SV) based estimation algorithms represent attractive methods for synchronized phasor, frequency and rate of change of frequency measurements in three-phase ac power systems. Recently, a phase-locked-loop (PLL) solution for improving the demodulation of the SV signal has been proposed. In this paper, the potentialities of the SV-PLL approach are investigated in order to optimize accuracy and computational load. First of all, the impact of the PLL update rate on achieved performance is analyzed. Then, a novel two-step SV-PLL algorithm is presented, so that the accuracy of a fast PLL execution frequency can be matched with a considerably lower computational cost. Behavior in case of fast phase angle variations has been also significantly improved. The proposed synchrophasor estimation technique has been validated through simulations; exemplary dynamic performance suggests that it is particularly suitable for grid control applications. Experimental tests carried out on a real-time implementation confirm simulation results.**

***Keywords*—phasor measurement units, synchrophasor estimation, frequency measurement, voltage measurement, current measurement, power transmission, power distribution, phase locked loops, three-phase systems.**

I. Introduction

Phasor Measurement Units (PMUs) are becoming widespread in new generation wide area monitoring systems for transmission grids thanks to their ability to measure synchronized phasors, frequency and Rate of Change of Frequency (ROCOF) [1]. PMUs return measurements with respect to coordinated universal time (UTC) and are therefore very promising tools for network control applications; their employment in future distribution grids is under investigation.

The synchrophasor standard IEC/IEEE 60255-118-1 [2] (which superseded the previous IEEE C37.118.1 [3] and its amendement [4]) defines accuracy limits for PMU compliance verification under both steady-state and dynamic conditions; it is based on simple test signals that allow covering the most significant operating scenarios. Two compliance classes are defined in [2] in order to distinguish between protection (class P) or measurement (class M) applications. The former requires fast response and low latency, while the latter demands for stronger disturbance rejection and larger bandwidth.

The increasing importance of PMUs and the challenges to be faced in their design have stimulated the interest of the scientific community, particularly about the digital signal processing algorithms that are key in obtaining very accurate estimates. Many proposals for synchrophasor, frequency and ROCOF estimation techniques have been presented in the last decade (see [5] for an overview). Several approaches have been employed: discrete fourier transform (DFT) [3], interpolated DFT (IpDFT) [6], iterative IpDFT [7], compressive sensing on DFT [8], high rate sampling and interpolated resampling [9], [10], cascade boxcar filtering [11], dual channel architecture for simultaneous class P and M compliance [12].

Recently, techniques that leverage the three-phase characteristics of electrical signals to improve estimates have been proposed in [13] and [14]; positive sequence synchrophasor, frequency and ROCOF measurements are computed by means of the space vector (SV) transformation. These papers use a reference frame which rotates at the rated angular frequency; thanks to the complex demodulation, measurements are obtained by filtering SV magnitude and phase angle. In [15], the SV in a stationary reference frame represents the input of the IpDFT algorithm. The negative frequency image component becomes extremely small in the SV signal, since in this case it is purely due to unbalance: long-range leakage is heavily mitigated and accuracy is considerably improved under off-nominal frequency conditions. However, it is important to recall that IpDFT is intrisically based on a steady-state model. Similarly, [16] combines the SV transformation with Taylor-Fourier filters, yielding to noticeable advantages both in terms of passband filter design flexibility and computational cost. This allows to cope with varying conditions, but within the limits imposed by a model that is exact only at nominal frequency. SV-based techniques have been proposed also by other researchers. In [17] the SV transformation on a stationary reference frame is applied to an artificial three-phase signal obtained from a single-phase waveform through sample shifts of one third of the rated cycle. The negative image component is suppressed like when the Hilbert transform is employed

Dr. Pegoraro work was partially funded by Fondazione di Sardegna for the research project "SUM2GRIDS, Solutions by mUltidisciplinary approach for intelligent Monitoring and Management of power distribution GRIDS".

R. Ferrero is with the Department of Electrical Engineering and Electronics, University of Liverpool, Liverpool, UK (e-mail: roberto.ferrero@liverpool.ac.uk).

P. A. Pegoraro is with the Department of Electrical and Electronic Engineering of the University of Cagliari, Piazza d'Armi, 09123 Cagliari, Italy (e-mail: paolo.pegoraro@unica.it).

S. Toscani is with Dipartimento di Elettronica, Informazione e Bioingegneria, Politecnico di Milano, Milan, Italy (e-mail: sergio.toscani@polimi.it).

[18]; therefore, it is not able to exploit the actual three-phase nature of power system quantities, which allows increasing accuracy and reducing computational burden simultaneously. It should be noticed that all these SV-based techniques rely on a reference frame which rotates at constant speed: this results in constraints about the minimum bandwidth of the filters that allows extracting the synchrophasor, thus decreasing disturbance rejection capabilities. From another perspective, frequency-tracking techniques have been used to deal with off-nominal frequency conditions and slow phase modulations [12], [19]. Phase locked loops (PLLs) can be used to measure synchrophasor [20], frequency [21] or to increase the performance of PMU algorithms based on Taylor-Fourier filters [22].

In [23], similarly to [13], three-phase demodulation is performed by means of Park transformation and IIR filtering; the angular position of the reference frame is the output of a digital PLL running at the sampling rate. In [24] a digital PLL is used to improve the SV-based measurement algorithms presented in [14]; phase-angle, frequency and ROCOF estimates at previous reporting time are exploited to update the position of the reference frame for all the input samples in the next observation window. Positive sequence synchrophasor, frequency and ROCOF estimates are obtained by filtering the amplitude and phase angle of the resulting SV signal. The relatively slow execution rate of the PLL (equal to the reporting rate) ensures moderate computational load.

In this paper, the combined employment of SV and digital PLL approaches is investigated and two new techniques are introduced. First, filters have been optimized for the needs of SV-PLL combination and the role of PLL update rate on overall performance is deeply analysed. Then, starting from the analysis outcomes, a two-step PLL solution which brings twofold advantages is proposed: it sligthly improves accuracy and, above all, it drastically reduces computational burden with respect to sample-by-sample PLL execution. From another point of view, it clearly enhances performance with respect to the algorithm presented in [24] while resulting in a moderate computational load, thus allowing easy real-time implementation. Abrupt changes in the input signal phase angle represent a major issue for PLL-based algorithms, however it is rarely investigated. A simple solution which allows dramatically improving performance under this condition is proposed and validated. Real-time implementation on a modular hardware has been carried out.

II. Background on SV Approach for Synchrophasor Estimation

The definition of dynamic synchrophasor relies on the following model for a generic electric signal in an ac power system:

$$x(t) = \sqrt{2}X(t)\cos(\omega_0 t + \varphi(t)) + d(t) \tag{1}$$

where $\omega_0 = 2\pi f_0$ is the rated angular frequency (with f_0 the rated system frequency, e.g. 50 Hz) and $d(t)$ includes all the harmonic and non-harmonic disturbances. $\bar{X}_S(t) = X(t)e^{j\varphi(t)}$ is the so-called dynamic synchrophasor associated with $x(t)$, describing the amplitude and phase-angle evolution of the fundamental component on a UTC synchronized timescale. PMU algorithms aim at measuring $\bar{X}_S(t)$ as well as the first and second order derivatives of its phase $\varphi(t)$, namely the instantaneous frequency deviation and ROCOF.

The input signal may undergo different conditions (off-nominal frequency, amplitude and phase modulations, frequency ramps, steps, etc.) and each of them requires peculiar features of the estimation algorithm for achieving accurate measurements. In addition, as shown in (1), $d(t)$ models disturbances which have to be properly mitigated. For these reasons, an estimation algorithm comes out as the result of a trade-off between conflicting requirements: large bandwith to preserve fundamental component dynamics and strong disturbance rejection.

Focusing on sinusoidal steady-state conditions characterized by angular frequency $\omega = 2\pi f$, the signal $x(t)$ can be described as ($'*'$ indicates the complex conjugate operator):

$$x(t) = \frac{1}{\sqrt{2}}\left[\bar{X}e^{j\omega t} + \bar{X}^* e^{-j\omega t}\right] \tag{2}$$

that is by means of the real part of $\bar{X}_S(t)e^{j\omega_0 t}$, where $\bar{X}_S(t) = \bar{X}e^{j(\omega-\omega_0)t}$.

In this simple but important case, synchrophasor can be computed, except for a simple phase angle rotation, by attenuating the image component of the sinusoid, which represents a strong harmonic disturbance at a distance of $2f$ from the positive frequency term. Its impact plays an important role in synchrophasor estimation and the SV approach is extremely effective in dealing with it when three-phase signals are concerned, as it will be recalled in the following.

Assuming that only the positive sequence synchrophasor of a three-phase quantity has to be estimated (along with frequency and ROCOF) the SV approach gives significant advantages [14]. Three-phase peculiarities are exploited and a direct computation of the positive sequence component is obtained. Given a generic three-phase signal:

$$\boldsymbol{x}_{abc}(t) = \begin{bmatrix} x_a(t) \\ x_b(t) \\ x_c(t) \end{bmatrix} \tag{3}$$

where $x_p(t)$ ($p \in \{a, b, c\}$) is the signal corresponding to phase p and each phase signal can be represented as in (1). The SV transformation on a generic reference frame characterized by its instantaneous angular position $\beta(t)$ is performed. The following expression gives the complex-valued SV signal $\bar{x}_{SV}$ which contains all the required information:

$$\bar{x}_{SV}(t) = \\ = \sqrt{\frac{2}{3}}\begin{bmatrix} 1 & \bar{\alpha} & \bar{\alpha}^2 \end{bmatrix}\boldsymbol{x}_{abc}(t)\, e^{-j\beta(t)} \tag{4}$$

where $\bar{\alpha} = e^{j2\pi/3}$.

In the conventional SV-based estimator (see [13] and [14]) $\beta(t) = \omega_0 t$, thus the reference frame performs a demodulation at the nominal frequency (that is a frequency shift towards baseband). Considering off-nominal frequency conditions as in (2), the SV can be written as [14]:

$$\bar{x}_{SV}(t) = \bar{X}_+ e^{j(\omega-\omega_0)t} + \bar{X}_-^* e^{-j(\omega+\omega_0)t} + \bar{d}_{SV}(t) \tag{5}$$

where $\bar{X}_+$ is the positive sequence component, $\bar{X}_-$ is the negative sequence component, and $\bar{d}_{SV}(t)$ is a complex-valued signal including harmonic and non-harmonic disturbances. It should be noticed that the zero sequence term does not appear into (5) since it is orthogonal with respect to the SV transformation [25]. The positive sequence synchrophasor can be defined as follows:

$$\bar{X}_{+,S}(t) = \bar{X}_+ e^{j(\omega-\omega_0)t} \tag{6}$$

Once again the synchrophasor (6) can be obtained from the SV signal by removing disturbances, and, in particular, the image component. It can be easily shown [13] that the latter corresponds to the conjugate of the negative sequence component $\bar{X}_-$ in the three-phase signal. Since unbalance level is typically small in power systems, $\bar{X}_-$ is noticeably smaller than $\bar{X}_+$, making the positive sequence synchrophasor extraction much easier than in the single-phase case (2).

When different conditions are considered, the model in (5) is slightly modified to include time-varying amplitude and phase angles, according to the definition of dynamic synchrophasor; it becomes a slowly varying bandbase signal which has to be preserved when ruling out disturbances.

In [14], proper filters are introduced as shown in Fig. 1 (subscript e indicates estimated quantities)[1]. First a lowpass filter H is applied to the SV signal; its role is removing most part of disturbances. Then, two FIR filters (M and P) are applied to the magnitude and phase of the resulting signal to obtain the positive-sequence synchrophasor amplitude and phase estimates. First and second order band limited FIR differentiators are designed to compute frequency and ROCOF from the phase angle of the filtered SV signal. Group delay introduced by the digital filters is kept into account in the timestamping process. It should be noticed that under balanced off-nominal frequency conditions, the real and imaginary parts of $\bar{x}_{SV}$, which are the inputs of filter H, are quadrature sinewaves at the angular frequency $\omega-\omega_0$. For this reason, the estimated magnitude may suffer from scalloping loss, namely attenuation under off-nominal frequency. As shown in Fig. 1, measured frequency is used to compensate for this effect, thus enabling very accurate estimates under off-nominal frequency conditions. Further details are available in [14].

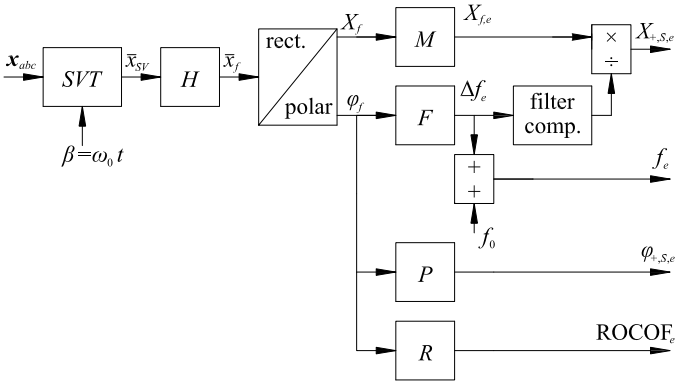

Fig. 1. Block diagram of SV-based PMU algorithms.

III. SV-PLL METHODS

A. SV-PLL technique at different execution rates.

The paper [24] proposed to exploit the estimated phase-angle, frequency, and, in some configurations, ROCOF at a given reporting instant to redefine the instantaneous position β of the reference frame in (4) for the samples belonging to the next observation window. Feedback was intended to operate at the PMU reporting rate, and thus the architecture in Fig. 1 was adapted accordingly.

In this paper, the limit of updating the reference frame instantaneous position at the PMU reporting rate is removed and a detailed description of the improved SV-PLL algorithm is reported.

Considering a sampling frequency f_s ($T_s = 1/f_s$ is the sampling interval) which is an integer multiple of the rated frequency so that $f_s = Mf_0$, M samples are acquired for each nominal cycle (20 ms for a 50 Hz system). Using the SV approach amplitude, phase angle, frequency and ROCOF estimations are performed by means of the cascade of two FIR filters; the minimum number N of samples needed for each computation depends on N_H, namely the number of taps of filter H, and N_{max}, which is the number of taps of the longest filter between M, P, F and R. Due to the cascade $N = N_H + N_{max} - 1$. In the following, filters are assumed to introduce a constant group delay $L = (N-1)T_s/2$ (odd N) for the sake of simplicity.

Fig. 2 shows the block diagram of the proposed algorithm. The incoming data is grouped into N-samples observation windows, each one generated every m samples. Therefore these windows are overlapped by $N-m$ samples and mT_s represents the delay of the feedback process that allows updating the angular position β.

By adopting this approach, measurements at instant $(k-1)mT_s$ are used to define the reference frame around instant kmT_s as follows:

$$\begin{aligned}\beta(kmT_s + nT_s) = \varphi_{+,S,e}((k-1)mT_s) + \\ + 2\pi f_e((k-1)mT_s)\,((m+n)T_s) + \\ + \pi \mathrm{ROCOF}_e((k-1)mT_s)\,((m+n)T_s)^2\end{aligned} \tag{7}$$

where k is the computation instant index and $n \in [-L, L]$ is the index spanning the SV samples in the observation window. Equation (7) expresses the phase angle forecast based on previous measurements $\varphi_{+,S,e}((k-1)mT_s)$, $f_e((k-1)mT_s)$ and $\mathrm{ROCOF}_e((k-1)mT_s)$. If the forecasted phase angle evolution is accurate, this translates into a more precise baseband demodulation. In addition, scalloping loss compensation is no longer necessary.

It is important to notice that (7) represents a second order Taylor expansion of the phase angle centered in the measurement instant $(k-1)mT_s$ having assumed constant ROCOF. When the last term is neglected, the first order PLL is obtained:

[1]The filtering scheme and the architecture of [14] are reported here for the sake of clarity and because the proposed architectures in Sections III and IV are based on similar concepts.

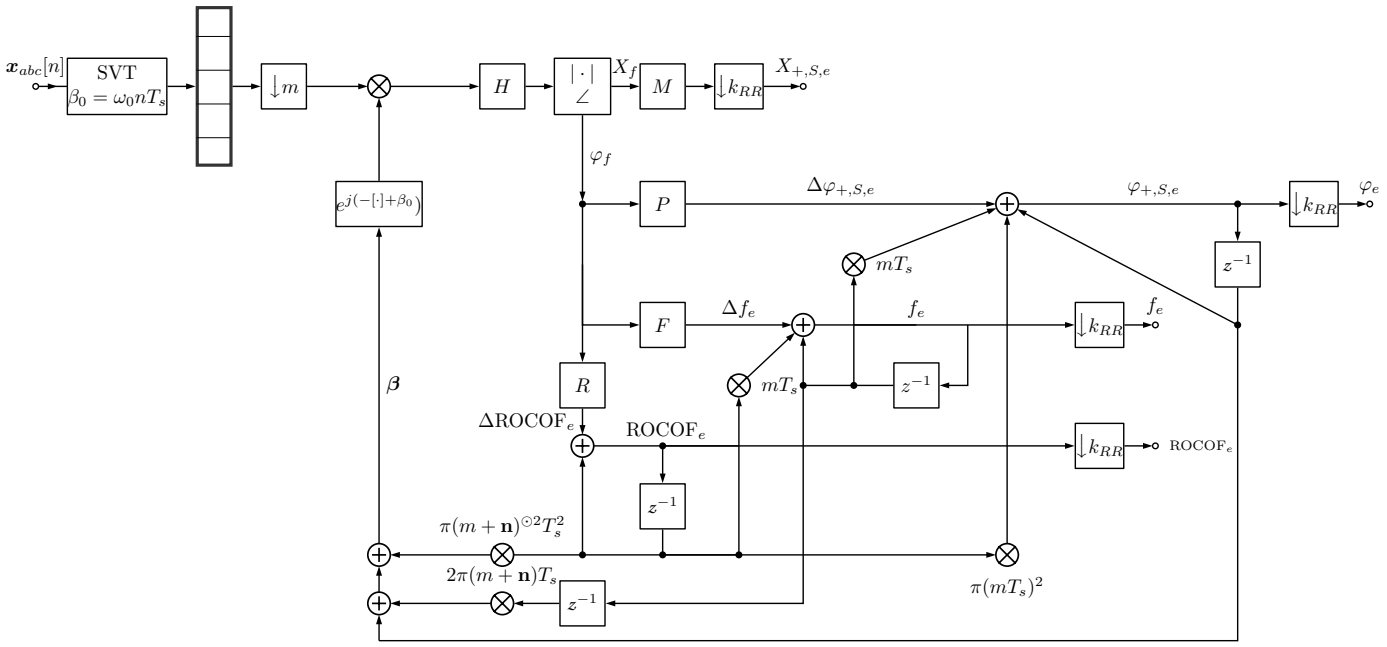

Fig. 2. Block diagram of the SV-PLL algorithm.

constant frequency is implicitly assumed when generating the instantaneous position of the reference frame. Intuitively a more effective demodulation is achieved when considering a smaller m, since the Taylor expansion is used over a shorter time interval corresponding to $m + L$ samples. However, the drawback is that a smaller m leads to a larger overlap between computation windows, thus considerably increasing the computational burden. The influence of this parameter has to be properly analysed in order to obtain an effective trade-off between accuracy and harware requirements.

In this new context, the improved demodulation thanks to the PLL should be exploited during filter design. First of all, lowpass filter P no longer requires a passband which is large enough to preserve all the phase angle dynamics. As an example, the frequency offset due to off-nominal conditions (e.g. in the range $[-2, 2]$ Hz for a P-class PMU in [2]) or the frequency variations due to phase-angle modulation (with a modulation frequency of few Hz), impose constraints on the in-band attenuation in order to achieve satisfactory performance. Thanks to the PLL, such requirements can be relaxed, thus allowing more freedom to achieve disturbance rejection.

Phase angle needs to be measured with respect to the nominal-frequency rotating frame, while the output of the filtering chain returns the phase angle deviation $\Delta\varphi_{+,S,e}$ with respect to the phase-locked reference frame. Therefore, the following coordinate change is needed:

$$\varphi_{+,S,e}(kmT_s) = \Delta\varphi_{+,S,e}(kmT_s) + \beta(kmT_s) - \omega_0 kmT_s - \theta_0 \quad (8)$$

where θ_0 is the initial phase of the rotating frame.

Frequency is obtained from the following expression:

$$f_e(kmT_s) = \Delta f_e(kmT_s) + \frac{1}{2\pi}\dot{\beta}(kmT_s) \quad (9)$$

where the computed frequency deviation $\Delta f_e(kmT_s)$ must be corrected by taking into account the instantaneous angular speed $\dot{\beta}$ of the reference frame. $\dot{\beta}$ is obtained from the continuous time expression of β and results:

$$\dot{\beta}(kmT_s) = 2\pi f_e((k-1)mT_s) + + 2\pi\text{ROCOF}_e((k-1)mT_s)\,(mT_s) \quad (10)$$

Finally, ROCOF can be obtained by the following expression that takes into account the variation of the rotational speed of the reference frame:

$$\text{ROCOF}_e(kmT_s) = \Delta\text{ROCOF}_e(kmT_s) + \text{ROCOF}_e((k-1)mT_s) \quad (11)$$

When the first order expansion is adopted for predicting β, the previous ROCOF correction is not needed since the rotational speed of the reference frame is constant.

Using the above architecture, estimates are available every mT_s seconds; PMU output measurements can be easily obtained via subsampling according to the considered reporting rate T_{RR}. Assuming $T_{RR} = M_{RR}T_s$, m is supposed to be a divisor of M_{RR}: for instance, if a reporting rate of 50 frames/s is used, $M_{RR} = M$ and $M = k_{RR}m$. As mentioned above, m is the result of a compromise between computational burden and accuracy.

In the following subsections, an analysis of the impact of window overlap is performed in order to show the potentialities and limitations of the method.

B. Implementation and filter design

The proposed SV-based phase tracking technique is particularly interesting as far as P class compliance has to be met. If constant group delay FIR filters are employed, their overall length has to be lower than four nominal cycles because of latency constraints [2]. In this respect, compliance tests include those with phase modulated (PM) signals that have to be carried out with modulation frequencies up to 2 Hz (50 Hz rated frequency and 50 phasors/s reporting rate are assumed). This means that the phase evolution has to be followed over a time window which is shorter than $4/25$ of a modulation period. Furthermore previous measurements are employed to generate the position of the reference frame that allows estimating phase, frequency and ROCOF after $mT_s \leq T_{RR}$, which is no more than $1/25$ of a modulation period. Because of these fairly short intervals we expect that using a second order expansion of the phase angle would allow an extremely effetive demodulation.

Now the target is investigating the advantages of using the proposed first and second order SV PLL (SV-PLL1 and SV-PLL2 respectively) at different execution rates with respect to the conventional SV technique. The implentations share the same filters that heavily impact on overall performance; the aim is achieving P-class compliance. As in the previous paragraph, f_0=50 Hz and 50 phasors/s are assumed. 10 kHz sampling frequency has been employed, while a target latency of L=300 samples (thus corresponding to 1.5 nominal cycles) has been considered. As an additional constraint, the algorithm is required to comply with P class limits for harmonic disturbances even when frequency deviates up to 1 Hz with respect to its rated value.

Constant group delay FIR filters are assumed, thus the design goal about latency translates in 601 coefficients for the cascade between the input filter H and those employed for magnitude, phase, frequency and ROCOF estimations. This means that the sum between the number of coefficients of the input filter and the highest among the others has to be equal to 602. ROCOF estimation is particularly sensitive to disturbances, namely 401 coefficients have been allocated for filter R, which is a second order differentiator. It has been designed as the cascade between two identical equiripple partial band differentiators characterized by 35 Hz stopband frequency. Design parameters have been tuned so that R has zeros close to multiples of f_0.

Coefficients are scaled in order to have zero error when estimating the second derivative of a parabolic input, which is a linearly increasing deviation between angular frequency and rotational speed of the reference frame. It should be noticed that the magnitude response of filter R is fairly flat at multiples of f_0 (zero derivatives); this allows achieving good harmonic disturbance rejection even under off-nominal frequency conditions.

Filter F has been designed as a 401-tap equiripple partial-band differentiator; since only a very narrow bandwidth is required in order to accurately follow the PM signals prescribed by [2] it is possible to achieve strong stopband attenuation; 35 Hz stopband frequency has been used. Coefficients are scaled so that zero error is achieved when estimating the slope of a phase ramp, which corresponds to a constant slip between space vector and reference frame. Filter M allowing magnitude estimation has been designed as a 401 tap equiripple low-pass filter having 2-Hz passband edge, 50-Hz stopband edge and 10^{-3} passband ripple in order to guarantee high accuracy under amplitude modulation in the most demanding conditions required by [2]; this resulted in 23.5 Hz -3dB cutoff frequency. Filter P used for phase estimation is an equiripple low-pass filter having the same order and passband ripple, but thanks to the features of the proposed techniques a lower passband edge (1 Hz, corresponding to 16.4 Hz -3dB cutoff frequency) can be used without sacrificing dynamic performance.

Thanks to the frequency tracking capability of the SV-PLL method or the scalloping loss compensation of the conventional SV approach, the bandwidth of filter H is not critical in off-nominal conditions; in order to further improve harmonic disturbance rejection, a 201 coefficient boxcar filter resulting in 22.1 Hz -3dB cutoff frequency has been chosen.

C. Off-nominal frequency and disturbance rejection

The conventional SV method and the proposed first and second order SV-PLL technique with different execution rates (according to the value of m) have been implemented and compared. Accuracy has been evaluated in terms of total vector error (TVE), frequency error (FE) and ROCOF error (RFE) as defined by the standard [2]. Considering off-nominal frequency conditions ($f \in [48, 52]$ Hz), numerical simulations show that, as expected from the considerations reported in Section II, all the methods exhibit negligible errors regardless the initial phase angle of the input signal. These errors are due only to numerical approximations and are not reported here for the sake of brevity.

SV-PLL techniques have similar noise rejection performance with respect to the conventional SV approach adopting the same filters. Considering a positive sequence input at the rated frequency and a typical 70 dB signal to noise ratio (SNR), the rms values of TVE, FE and RFE are $0.0016\,\%$, 0.094 mHz and 0.013 Hz/s respectively; these errors are inversely proportional to the SNR.

All the analyzed techniques share the same performance also under the other considered steady-state tests under rated frequency conditions; assuming small frequency and ROCOF estimation errors, the SV-PLL approach behaves like the conventional SV method. Applying a positive sequence input at the rated frequency f_0 while superimposing a $1\,\%$ positive sequence harmonic disturbance results in TVE, FE and RFE values which are below $1.4 \cdot 10^{-4}\,\%$, 0.073 mHz and $1.3{\cdot}10^{-3}$ Hz/s. Maximum values are reached for a second order harmonic disturbance, thus representing the most demanding condition. Dc rejection has been investigated by adding a three-phase dc term having zero sum (homopolar term does not affect the SV) and $1\,\%$ three phase rms amplitude to the main positive sequence term at the rated frequency. This results in a disturbance having frequency f_0 in the real and imaginary parts of the SV, namely identical to that produced by a positive

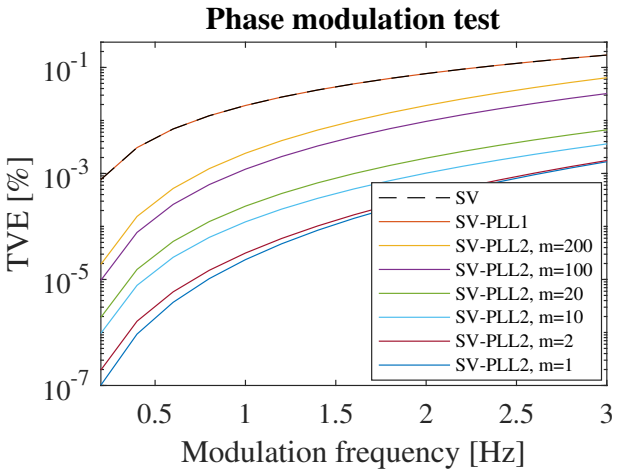

Fig. 3. Maximum TVE achieved by the different SV-based algorithms, PM test.

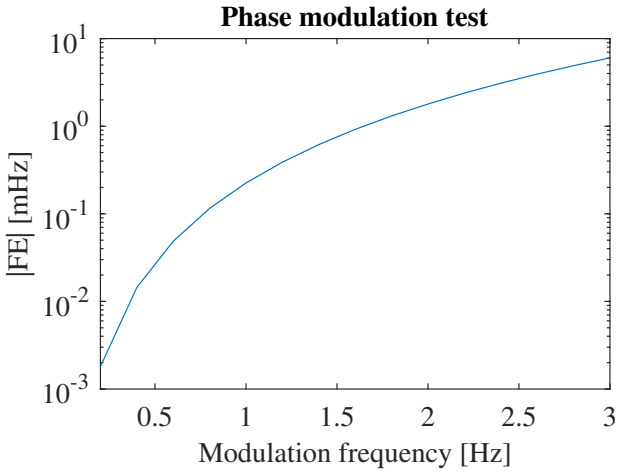

Fig. 4. Maximum FE achieved by the different SV-based algorithms, PM test.

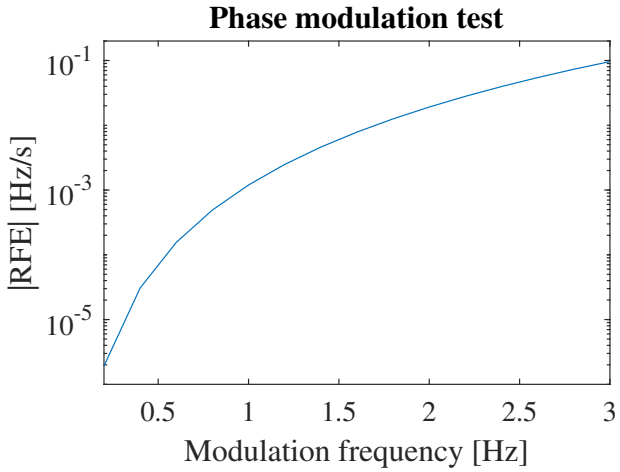

Fig. 5. Maximum RFE achieved by the different SV-based algorithms, PM test.

sequence second order harmonic [14]. For this reason, TVE, FE and RFE are the same as the maximum values achieved during harmonic disturbance test.

Finally, a $1\,\%$ of negative sequence component has been added to the positive sequence term at frequency f_0. SV-based methods show exemplary performance also under unbalanced input [26]: $1.2 \cdot 10^{-4}\,\%$ TVE, $0.032\,$mHz FE and $2 \cdot 10^{-4}\,$Hz/s RFE. It can be easily shown that these values are identical to those produced by a positive sequence third order harmonic disturbance having the same amplitude.

D. Dynamic performance

Having investigated the steady-state accuracy of the proposed SV-PLL techniques, now the focus is moved on dynamic performance. First of all, PM signals have been considered; their generic expression is:

$$x_p(nT_s) = \sqrt{2}X_1 \cdot \\ \cdot \cos\left(2\pi f_0 nT_s + \psi_p + k_a \cos\left(2\pi f_m nT_s - \pi\right)\right) \tag{12}$$

where $p \in \{a, b, c\}$ denotes the system phase while ψ_p is $0, -\frac{2}{3}\pi, +\frac{2}{3}\pi$ depending on the considered phase. These signals are useful to test the tracking capabilities of the algorithms, since frequency and ROCOF are time-dependent quantities (cosinusoidal functions of time). $k_a = 0.1$ is considered as in the compliance tests of [2], while modulation frequencies f_m between 0.2 Hz and 3 Hz have been employed to explore the limits and stress the algorithms. Results are summarized in Figs. 3-5.

When looking at Fig. 3 it should be noticed that the conventional SV and the SV-PLL1 techniques achieve the same accuracy in estimating the synchrophasor, thus reaching a maximum TVE value above $0.17\,\%$ (well below the $3\,\%$ limit) at the maximum considered modulation frequency. The reason is that when a first order Taylor expansion is employed to generate the instantaneous position of the reference frame, it is not capable to follow the phase-angle dynamics of PM signals, but only constant frequency deviations; performance are also not affected by changing the execution rate of the PLL. Adopting a second order PLL permits remarkably better accuracy since the reference frame becomes capable of tracking the phase angle modulation: maximum TVE is more than halved with $m = 200$ (thus when the PLL is executed at the reporting rate). Increasing the speed of the PLL allows a further, significant reduction of TVE, which falls below $4 \cdot 10^{-4}\,\%$ with $m = 10$ and below $2 \cdot 10^{-4}\,\%$ with $m = 1$. Of course, also the computational burden is considerably increased in the last case.

In Figs. 4, 5 only a trace is reported: FE and RFE values achieved by both the SV-PLL1 and SV-PLL2 are not affected by the execution rate. They are well below the P-class compliance limits and exactly the same as those obtained with the conventional SV method. Also in this case, the reason is simple: a reference frame whose angular position is a second order polynomial is not capable of properly follow the frequency dynamics, since the angular acceleration is supposed

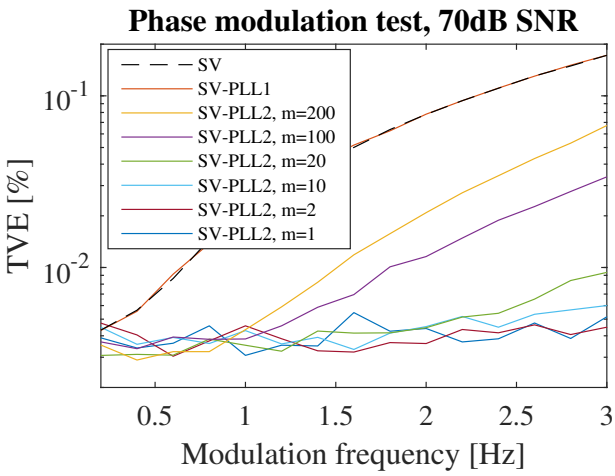

Fig. 6. Maximum TVE achieved by the different SV-based algorithms, PM test, 70dB SNR.

to be constant. Therefore there is no advantage in adopting the SV-PLL2 algorithm with respect to the conventional SV method or to the SV-PLL1 that uses a reference frame having constant rotational speed over the observation window. Similar considerations applies to ROCOF estimation.

The previous results highlight that using the SV-PLL2 method with fast PLL execution rates allows more accurate synchrophasor measurements with PM input signals. However, since the drawback is a considerable increase of the computational burden, it should be investigated if these performance improvements are masked by noise. Therefore PM tests are repeated with superimposed white noise corresponding to -70 dB signal to noise ratio (SNR); results are reported in Fig. 6. Maximum TVE values show that even considering a realistic SNR, using a fast second order PLL allows a much better accuracy. This means that the impact of noise is well below the error contirbution due to the algorithms, at least when $m \geq 10$; however, further increasing the PLL execution speed ($m = 1$ or 2) does not provide significant performance gain.

Considering frequency ramp tests with ± 1 Hz/s slope, the conventional SV approach results in a very low maximum TVE equal to $0.031\,\%$, exactly the the same as that obtained with the SV-PLL1 method. TVE becomes absolutely negligible when the SV-PLL2 technique is adopted, since the predictor used to generate the reference frame angular position is exact under this condition. It is worth mentioning that all the SV-based techniques achieve virtually zero FE and RFE.

As for the performance under transient conditions, it is significant to discuss results considering step changes, as suggested by the standard. In particular, a magnitude step change does not affect the estimated phase (and hence also frequency and ROCOF which are related to their derivatives). For this reason, as it can be noticed from [14, Tables II and IV], SV-based phase, frequency and ROCOF estimations have theoretically zero error in this case. For this reason, introducing a PLL does not have effect on the estimations. Therefore, SV-PLL methods behave exactly like the conventional SV based

TABLE I. PHASE STEP RESPONSE RESULTS.

Index	**SV**	**SV-PLL1**	**SV-PLL2**					
			m=200	m=100	m=20	m=10	m=2	m=1
TVE resp [ms]	31.6	31.6	56.4	43.8	20	19.5	19.3	19.3
FE resp [ms]	59	59	59	59	59	59	59	59
RFE resp [ms]	60	60	60	60	60	60	60	60
overshoot [ms]	0	0	12.1	10.3	5.6	4.0	4.3	4.3
delay [ms]	-0.1	-0.1	1.8	2.4	0.4	0.2	0.0	-0.1

algorithm. On the other side, PLLs typically suffer when the phase of the input signal exhibits an abrupt phase change, as in the phase step tests required by [2]. In this case, the expressions of the three input signals are:

$$x_p(nT_s) = \sqrt{2}X_1 \cos\left(2\pi f_0 n T_s + \psi_p + k_a u(t)\right) \qquad (13)$$

where $u(t)$ is the unit step function while k_a is the step amplitude, equal to $-\pi/18$. The procedure recommended by [2] has been implemented: an equivalent phasor sampling frequency of 10 kHz has been obtained by applying M steps at different, evenly spaced instants with respect to the reporting time and by interleaving the obtained response samples based on corresponding time shifting. As expected, all the implementations are characterized by the same FE and RFE response times (59 ms and 60 ms, respectively) and zero delay times. However, significant differences emerge in terms of TVE response times and phase overshoots, as it can be noticed from Table I.

Performance indexes are identical for the conventional SV algorithm and the SV-PLL1 method, which also in this case is not affected by the execution rate of the PLL (only one column is reported in Table I). Conversely, results obtained with SV-PLL2 strictly depend on m. In particular, when the parameters used to generate the reference frame are updated at the reporting instants ($m = 200$), the TVE response time increases to 56 ms and the phase estimate shows a large overshoot above $12\,\%$: P class compliance is not met in this case. Decreasing the value of m yields to a consistent reduction of the TVE response time down to 19.3 ms, considerably lower than the conventional SV method. Also the overshoot becomes much smaller ($4.3\,\%$) but it is marginally better than the $5\,\%$ compliance limit and far worse than that obtained by using the SV method without PLL.

IV. TWO-STEP SV-PLL

A. Improved SV-PLL approach

The results presented in III-D highlight that using a second order PLL in conjunction with the SV approach yields a remarkable accuracy improvement in estimating the synchrophasor under dynamic conditions (PM signals), especially when a fast execution rate is employed. The drawbacks are that the computational cost increases with the rate and that there are no advantages as far as frequency and ROCOF measurements are concerned.

This last observation can be exploited in order to significantly reduce the computational burden, without sacrificing

accuracy in synchrophasor estimation; in particular, the architecture in Fig. 7 can be adopted.

Let us suppose to have available phase, frequency and ROCOF estimates in the previous reporting instant. The instantaneous position β of the reference frame for the next measurement in $t = kT_{RR}$ is first of all generated as in the SV-PLL2 with $m = M_{RR}$, hence using (7). Frequency and ROCOF estimates $f_e(kT_{RR})$ and $\text{ROCOF}_e(kT_{RR})$ can be computed using filters H, F and R and they can be used to refine the instantaneous position of the reference frame β, so that the second order Taylor expansion is now centered in the reporting instant, unlike the solution proposed in Section III-A. Then, the following expression holds for β:

$$\begin{aligned}\beta(kmT_s + nT_s) = \varphi_{+,S,e}((k-1)mT_s) + \\ + 2\pi f_e(kmT_s)\,(nT_s) + \\ + \pi \text{ROCOF}_e(kmT_s)\,(nT_s)^2 \end{aligned} \quad (14)$$

where phase angle dynamics are described around current reporting instant, resulting in a better approximation. The phase angle at the centre of the window is not crucial since it can result in a simple offset, which does not affect the final result. Synchrophasor measurement is performed in this reference frame which allows a very effective baseband demodulation with a computational burden which is similar to that of the SV-PLL2 method with $m = M_{RR}/2$.

The other drawback of the SV-PLL2 synchrophasor estimator is the large overshoot which occurs when the phase angle exhibits abrupt changes. The reason is related to the large and slowly-damped ROCOF error which enters in the PLL. In order to overcome this issue, the idea is limiting the dynamics of the reference frame instantaneous position; of course, this should not jeopardize the performance achieved with PM signals.

First of all, it has been introduced a saturation on the variation which the ROCOF used to generate the reference frame may undergo. In order to not affect demodulation under PM conditions, this maximum change dROCOF_{th} has been selected according to the following expression:

$$\text{dROCOF}_{th} = (2\pi)^2 k_{a,max} f_{m,max}^3 T_{RR} \quad (15)$$

Parameter dROCOF_{th} is a threshold value which takes into account highly dynamic but realistic conditions, so that abrupt changes in the phase locked reference frame are contained. Basically, it takes into account the maximum ROCOF derivative in the considered PM signals; in fact, $f_{m,max}$ is chosen as the maximum modulation frequency while $k_{a,max}$ is the maximum amplitude of phase angle modulation within the considered interval T_{RR}.

Furthermore, a saturation in the absolute value of the ROCOF used to generate the reference frame is added. The saturation threshold ROCOF_{th} has been selected according to the following expression, thus ensuring that PM peformance is not jeopardized for given $f_{m,max}$ and $k_{a,max}$.

$$\text{ROCOF}_{th} = 2\pi k_{a,max} f_{m,max}^2 \quad (16)$$

It should be noticed that this saturation on the ROCOF used to generate the reference frame does not prevent the capability of measuring ROCOF values exceeding ROCOF_{th}.

B. Tests and results

The 2-step SV-PLL (2S SV-PLL) method introduced in Section IV-A has been implemented by using the same nominal frequency, reporting rate, sampling frequency and filter designs that have been previously defined in Section III-B. Saturation thresholds dROCOF_{th} and ROCOF_{th} have been obtained by assuming $f_{m,max} = 3\text{Hz}$ and $k_{a,max} = 0.1$.

First of all, performance under PM has been evaluated by considering $f_m \in [0.2, 3]\,\text{Hz}$ and $k_a = 0.1$. The achieved TVE is almost identical (marginally better) to that obtained by adopting the second order PLL with $m = 1$: maximum TVE with $f_m = 3\,\text{Hz}$ is $1.6 \cdot 10^{-3}\,\%$. This represents a noticeable achievement, since computational burden is dramatically lower as long as the 2S SV-PLL algorithm is adopted. Noise rejection is the same exhibited by the other SV-based methods.

Phase angle step tests defined by [2] have been performed; Fig. 8 compares the phase estimates obtained with the different SV-PLL methods. Without engaging the saturation of the ROCOF used to generate the PLL reference frame, the 2S SV-PLL method results in almost the same performance of the SV-PLL2 approach with $m = 1$. The trend of the estimated phase (not shown in Fig. 8) is virtually identical to that obtained with SV-PLL2, thus characterized by negligible delay, fast response but a significant 4.2% overshoot. In fact, the behaviour of the SV-PLL algorithms is clearly influenced by the istantaneous position of the reference frame, which is affected by the ROCOF error occurring during the transient. Reducing the update rate helps in mitigating the initial overshoot, but it introduces a longer tail and undershoot in the response (yellow line) due to prolonged prediction errors. When the ROCOF employed in the PLL is saturated according to what described in Section IV-A, the plot of the phase estimated with the 2S SV-PLL technique becomes quite similar to that obtained with the conventional SV approach. This effect is the result of an increased immunity to large ROCOF deviations that prevents larger errors from propagating through the PLL. The TVE response time increases from 19.4 ms to 30.2 ms (similar to the 31.6 ms of the conventional SV method) but overshoot is lower than 1%.

Finally, the practical implementation of the proposed algorithms has been tested by using a real-time modular platform made of: a NI CompactRIO 9039 controller, a NI-9225 24 bit input module having 3 simultaneous sampling channels with 300 Vrms range [27] and a NI-9467 GPS synchronization module [28]. The characterization of the prototype have been performed using an OMICRON CMC 256plus synchronized generator [**?**], which is a high precision relay test set and universal calibrator characterized by typical accuracy equal to $0.015\,\%$ of reading plus $0.005\,\%$ of range for the voltage amplitude and of 0.005° and $0.5\,\text{ppm}$ for phase angle and frequency, respectively. The timebase error is below $1\,\mu\text{s}$ since IRIG-B synchronization with OMICRON CMIRIG-B [29] is adopted. Several tests have been performed and the results in

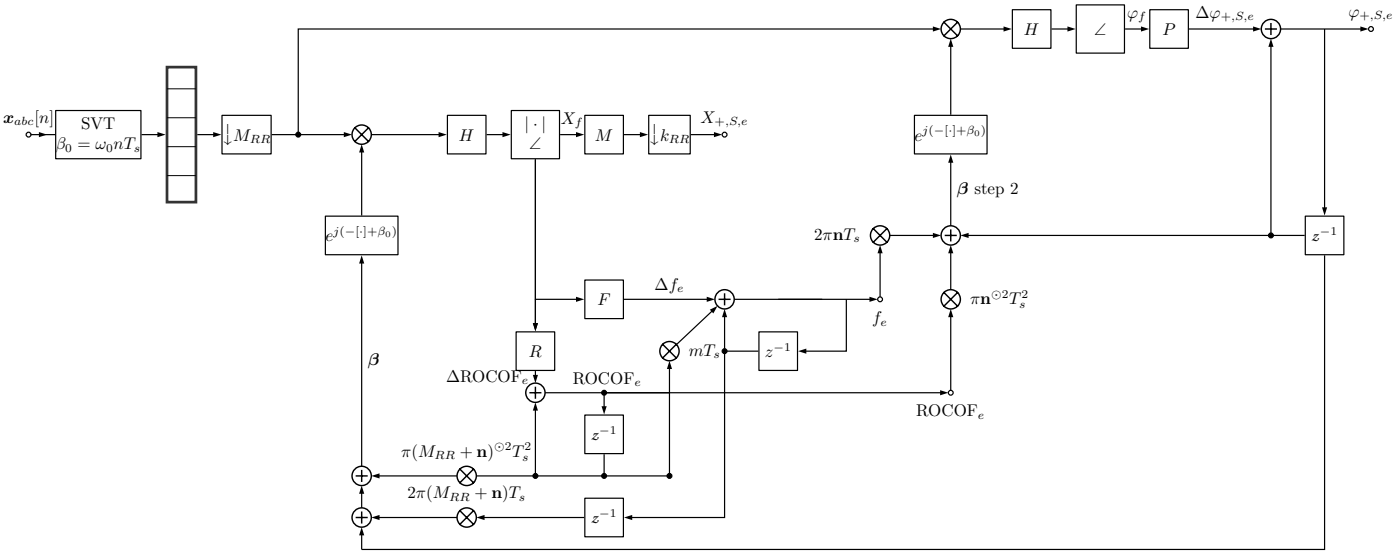

Fig. 7. Block diagram of the two-step SV-PLL algorithm.

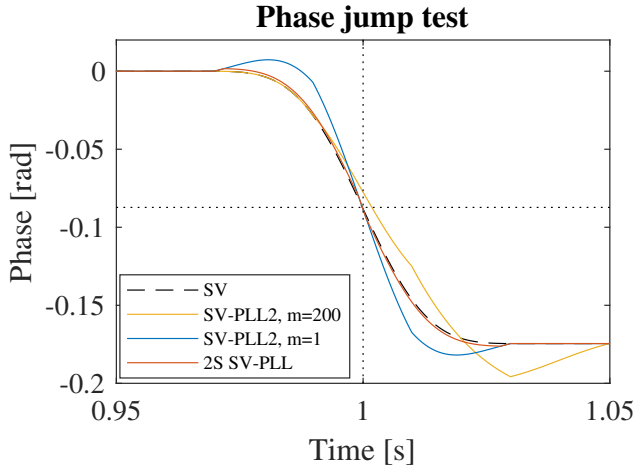

Fig. 8. Phase step responses of the different SV-based algorithms.

terms of estimation errors are compatible with the outcomes of the simulations. As an example, using the 2S SV-PLL method to measure a 3-phase 100 Vrms steady-state input signal during a 6-minute test (18000 measurements at 50 frames/s) the rms values of amplitude and phase angle errors are, respectively, $1.6 \cdot 10^{-4}$ % and $2.5 \cdot 10^{-3}$°, while FE and RFE rms values are about 0.07 mHz and 0.0025 Hz/s, respectively, thus in agreement with simulations results when also the uncertainty of the characterization chain is taken into account. Finally, to assess the performance of the prototype implementation also under dynamic conditions, a 5-s PM test with $f_m = 2$ Hz leads to rms values of amplitude and phase angle errors that are, respectively, $3.6 \cdot 10^{-3}$ % and $3.1 \cdot 10^{-3}$°; FE and RFE rms values are 7 mHz and 0.087 Hz/s, respectively, thus confirming again the feasability of proposed solution in a real platform and validating the prototype with the proposed algorithm while operating in real-time.

V. Conclusions

The paper has discussed PLL solutions which can be employed in conjunction with SV-based positive-sequence synchrophasor, frequency and ROCOF estimation algorithms for PMU applications in three-phase systems. The role of the expansion order which is employed to generate the instantaneous position of the reference frame and its update rate have been investigated in detail. The analysis has shown that unlike synchrophasor estimation, frequency and ROCOF measurements are not affected by the employed phase-locked reference frame. Starting from this result, a novel two-step algorithm can be adopted: it allows improving synchrophasor estimation without requiring a fast update of the reference frame used by the demodulation stage. Remarkable estimation accuracy under off-nominal frequency has been obtained along with excellent tracking capabilities of the typical electric signal dynamics and limited computation overhead. In addition, a simple but effective solution to deal with abrupt changes in the input signal phase angle has been proposed, so that the algorithm step response is not adversely affected by the PLL. The method has been implemented in a real-time modular platform, and experimental results confirm the performance achieved in numerical simulations.

Acknowledgements

Dr. Pegoraro work was partially funded by Fondazione di Sardegna for the research project “SUM2GRIDS, Solutions by mUltidisciplinary approach for intelligent Monitoring and Management of power distribution GRIDS”.

REFERENCES

[1] AA. VV., *Phasor Measurement Units and Wide Area Monitoring Systems*, 1st ed., A. Monti, C. Muscas, and F. Ponci, Eds. Academic Press, 2016.

[2] *IEEE/IEC International Standard - Measuring relays and protection equipment - Part 118-1: Synchrophasor for power systems - Measurements*, IEEE/IEC IEC/IEEE 60255-118-1:2018, Dec 2018.

[3] *IEEE Standard for Synchrophasor Measurements for Power Systems*, IEEE IEEE Std C37.118.1-2011 (Revision of IEEE Std C37.118-2005), Dec. 2011.

[4] *IEEE Standard for Synchrophasor Measurements for Power Systems – Amendment 1: Modification of Selected Performance Requirements*, IEEE IEEE Std C37.118.1a-2014 (Amendment to IEEE Std C37.118.1-2011), Apr. 2014.

[5] C. Muscas and P. A. Pegoraro, "Algorithms for synchrophasors, frequency, and rocof," in *Phasor Measurement Units and Wide Area Monitoring Systems*, 1st ed., A. Monti, C. Muscas, and F. Ponci, Eds. Elsevier, Academic Press, 2016, ch. 3, pp. 21–51.

[6] D. Belega and D. Petri, "Accuracy analysis of the multicycle synchrophasor estimator provided by the interpolated DFT algorithm," *IEEE Trans. Instrum. Meas.*, vol. 62, no. 5, pp. 942–953, May 2013.

[7] A. Derviškadić, P. Romano, and M. Paolone, "Iterative-interpolated DFT for synchrophasor estimation: A single algorithm for P- and M-class compliant PMUs," *IEEE Transactions on Instrumentation and Measurement*, vol. 67, no. 3, pp. 547–558, Mar. 2018.

[8] M. Bertocco, G. Frigo, C. Narduzzi, and F. Tramarin, "Resolution enhancement by compressive sensing in power quality and phasor measurement," *IEEE Trans. Instrum. Meas.*, vol. 63, no. 10, pp. 2358–2367, Oct. 2014.

[9] A. Carta, N. Locci, C. Muscas, and S. Sulis, "A flexible gps-based system for synchronized phasor measurement in electric distribution networks," *IEEE Trans. Instrum. Meas.*, vol. 57, no. 11, pp. 2450–2456, Nov. 2008.

[10] J. Kitzig, S. Schlaghecke, and G. Bumiller, "Power quality measurement system with pmu functionality based on interpolated sampling," *IEEE Trans. Instrum. Meas.*, vol. 68, no. 4, pp. 1014–1025, Apr. 2019.

[11] A. J. Roscoe, I. F. Abdulhadi, and G. M. Burt, "P and M class phasor measurement unit algorithms using adaptive cascaded filters," *IEEE Trans. Power Del.*, vol. 28, no. 3, pp. 1447–1459, Jul. 2013.

[12] P. Castello, J. Liu, C. Muscas, P. A. Pegoraro, F. Ponci, and A. Monti, "A fast and accurate PMU algorithm for P+M class measurement of synchrophasor and frequency," *IEEE Trans. Instrum. Meas.*, vol. 63, no. 12, pp. 2837–2845, Dec. 2014.

[13] S. Toscani and C. Muscas, "A space vector based approach for synchrophasor measurement," in *Instrum. and Meas. Technol. Conf. (I2MTC) Proc., 2014 IEEE Int.*, May 2014, pp. 257–261.

[14] S. Toscani, C. Muscas, and P. A. Pegoraro, "Design and performance prediction of space vector-based pmu algorithms," *IEEE Trans. Instrum. Meas.*, vol. 66, no. 3, pp. 394–404, Mar. 2017.

[15] R. Ferrero, P. A. Pegoraro, and S. Toscani, "Employment of interpolated DFT-based pmu algorithms in three-phase systems," in *Proc. of the IEEE Int. Workshop on Appl. Meas. for Power Syst. (AMPS)*, Liverpool, UK, Sep. 2017.

[16] P. Castello, R. Ferrero, P. A. Pegoraro, and S. Toscani, "Space vector taylor–fourier models for synchrophasor, frequency, and rocof measurements in three-phase systems," *IEEE Trans. Instrum. Meas.*, vol. 68, no. 5, pp. 1313–1321, May 2019.

[17] L. Zhan, Y. Liu, and Y. Liu, "A Clarke transformation-based DFT phasor and frequency algorithm for wide frequency range," *IEEE Trans. Smart Grid*, vol. 9, no. 1, pp. 67–77, Jan. 2018.

[18] G. Frigo, A. Derviškadić, and M. Paolone, "Reduced leakage synchrophasor estimation: Hilbert transform plus interpolated DFT," *IEEE Trans. Instrum. Meas.*, vol. 68, no. 10, pp. 3468–3483, Oct. 2019.

[19] A. Roscoe, "Exploring the relative performance of frequency-tracking and fixed-filter phasor measurement unit algorithms under C37.118 test procedures, the effects of interharmonics, and initial attempts at merging P-class response with M-class filtering," *IEEE Trans. Instrum. Meas.*, vol. 62, no. 8, pp. 2140–2153, Aug. 2013.

[20] M. Karimi-Ghartemani, B.-T. Ooi, and A. Bakhshai, "Application of enhanced phase-locked loop system to the computation of synchrophasors," *IEEE Trans. Power Del.*, vol. 26, no. 1, pp. 22–32, Jan. 2011.

[21] A. Carboni and A. Ferrero, "A Fourier transform-based frequency estimation algorithm," *IEEE Trans. Instrum. Meas.*, vol. 67, no. 7, pp. 1722–1728, Jul. 2018.

[22] J. A. de la O Serna, "Synchrophasor measurement with polynomial phase-locked-loop Taylor-Fourier filters," *IEEE Trans. Instrum. Meas.*, vol. 64, no. 2, pp. 328–337, Feb. 2015.

[23] F. Messina, P. Marchi, L. R. Vega, C. G. Galarza, and H. Laiz, "A novel modular positive-sequence synchrophasor estimation algorithm for pmus," *IEEE Trans. Instrum. Meas.*, vol. 66, no. 6, pp. 1164–1175, Jun. 2017.

[24] R. Ferrero, P. A. Pegoraro, and S. Toscani, "A space vector phase-locked-loop approach to synchrophasor, frequency and rocof estimation," in *Instrum. and Meas. Technol. Conf. (I2MTC) Proc., 2019 IEEE Int.*, May 2019, pp. 1–6.

[25] A. Ferrero and G. Superti-Furga, "A new approach to the definition of power components in three-phase systems under nonsinusoidal conditions," *IEEE Trans. Instrum. Meas.*, vol. 40, no. 3, pp. 568–577, June 1991.

[26] P. Castello, R. Ferrero, P. A. Pegoraro, and S. Toscani, "Effect of unbalance on positive-sequence synchrophasor, frequency, and rocof estimations," *IEEE Trans. Instrum. Meas.*, vol. 67, no. 5, pp. 1036–1046, May 2018.

[27] National Instruments. NI-9225 manual. Accessed: Oct. 2019. [Online]. Available: http://www.ni.com/pdf/manuals/374707e.pdf.

[28] ——. NI-9467 manual. Accessed: Sep. 2019. [Online]. Available: http://www.ni.com/pdf/manuals/373230c.pdf.

[29] OMICRON. CMIRIG-B. Accessed: Sep. 2019. [Online]. Available: https://www.omicronenergy.com/en/products/cmirig-b/.

Roberto Ferrero (S'10-M'14-SM'18) received his PhD degree (cum laude) in Electrical Engineering from Polytechnic of Milan, Italy, in 2013. From 2015 to 2019 he was a Lecturer with the Department of Electrical Engineering and Electronics, University of Liverpool, UK, where he is currently a Senior Lecturer (Associate Professor). His main research activity is focused on electrical measurements, particularly applied to power systems and electrochemical devices. He is a member of the IEEE Instrumentation and Measurement Society, and of its TC 39 (Measurements in Power Systems). He has been an Associate Editor of the IEEE Transactions on Instrumentation and Measurement since 2017.

Paolo Attilio Pegoraro (M'06-SM'19) received the M.S. (summa cum laude) degree in telecommunications engineering and the Ph.D. degree in electronic and telecommunications engineering from the University of Padova, Padua, Italy, in 2001 and 2005, respectively. From 2015 to 2018 he was an Assistant Professor with the Department of Electrical and Electronic Engineering, University of Cagliari, Cagliari, Italy, where he is currently Associate Professor. He has authored or co-authored over 100 scientific papers. His current research interests include the development of new measurement techniques for modern power networks, with attention to synchronized measurements and state estimation. Dr. Pegoraro is a member of IEEE Instrumentation and Measurement Society TC 39 (Measurements in Power Systems) and of IEC TC 38 (Instrument Transformers). He is an Associate Editor of the IEEE Transactions on Instrumentation and Measurement.

Sergio Toscani (S'08, M'12, SM'19) received the M.Sc. and the Ph.D degree (cum laude) in electrical engineering from the Politecnico di Milano, Milan, Italy, in 2007 and 2011 respectively. Since 2011 he is Assistant Professor in Electrical and Electronic Measurement with the Dipartimento di Elettronica, Informazione e Bioingegneria of the same University. His research activity is mainly focused on development and testing of current and voltage transducers, measurement techniques for powers systems, electrical components and systems diagnostics. Dr. Sergio Toscani is member of the IEEE Instrumentation and Measurement Society and of the TC-39 - Measurements in Power Systems.